metals

MDPI

Article

Transformation of the δ-Ferrite in SS2343 Austenitic Stainless Steel upon Annealing at 1050 °C, 1150 °C and 1250 °C

Boštjan Arh *, Franc Tehovnik and Franci Vode

Laboratory of Process Metallurgy, Institute of Metals and Technology (IMT), Lepi pot 11, 1000 Ljubljana, Slovenia; franc.tehovnik@imt.si (F.T.); franci.vode@imt.si (F.V.)

* Correspondence: bostjan.arh@imt.si; Tel.: +386-1470-1973

Abstract: The solidification behaviors of laboratory cast austenitic SS2343 stainless steel in terms of the volume fraction of δ-ferrite in the as-cast state and its transformation after subsequent annealing were investigated. Monitoring of morphological transformations of δ-ferrite in the microstructure show the progress of δ-ferrite dissolution. Annealing tests were conducted at 1050 °C, 1150 °C and 1250 °C with soaking times of 5 and 40 min. The thermodynamic prediction and metallographic identification of δ-ferrite are presented. The ferrite fractions were measured using a magnetic method and determined to be in the range between 10.7% and 14.6%. The volume share of δ-ferrite decreased with an increase in temperature and the time of annealing. About 50–55% the δ-ferrite was effectively transformed. The δ-ferrite phase, originally present in a dendritic morphology, tends to break up and spheroidize. The morphology varies from vermicular, lacy and acicular shapes to globular for higher temperatures and for longer exposure times. In the δ-ferrite after annealing, concentrations of Cr and Mo decrease, and conversely the concentration of Ni increase, all by small, but significant, amounts. The observed changes in the solute concentration can be explained in terms of the transformation of ferrite into austenite and sigma phases.

Keywords: austenitic stainless steel; delta ferrite; annealing; transformation; morphology

check for updates

Citation: Arh, B.; Tehovnik, F.; Vode, F. Transformation of the δ-Ferrite in SS2343 Austenitic Stainless Steel upon Annealing at 1050 °C, 1150 °C and 1250 °C. *Metals* **2021**, *11*, 935. https://doi.org/10.3390/met11060935

Academic Editor: Silvia Barella

Received: 7 May 2021
Accepted: 6 June 2021
Published: 9 June 2021

Publisher's Note: MDPI stays neutral with regard to jurisdictional claims in published maps and institutional affiliations.

Copyright: © 2021 by the authors. Licensee MDPI, Basel, Switzerland. This article is an open access article distributed under the terms and conditions of the Creative Commons Attribution (CC BY) license (https://creativecommons.org/licenses/by/4.0/).

1. Introduction

Austenitic stainless steels have numerous applications since they have a good combination of properties, such as corrosion and oxidation resistance, toughness, weldability, and mechanical strength at low and high temperatures. The properties and performance of austenitic stainless steels are closely related to their microstructures, especially the amount and distribution of delta-(δ–)ferrite, which, in the case of castings, depend mainly on the chemical composition and the cooling rate during solidification [1–7]. Although expected to be fully austenitic at room temperature, the as-cast microstructure of austenitic stainless steels generally contains a small amount of residual δ–ferrite. The presence of this δ–ferrite is detrimental to the hot ductility and can lead to cracks appearing either at the edges of the hot-rolled product as open cracks or on the surfaces of the finished product as silver defects containing oxides [4].

The solidification sequence of stainless steels is usually predicted using the Fe-Cr-Ni phase diagram [4]. The projection of the liquidus, ferrite solidus and austenite solidus lines in the Fe-Cr-Ni ternary diagram shows a peritectic reaction, L + α → γ for the Fe-Ni system of the phase diagram. The peritectic behavior continues until the liquidus line crosses the austenite solidus line, after which the reaction becomes eutectic: liquid → α + γ for the Cr-Ni system [4]. The initial solidifying phase is determined by the position of the alloy with respect to the liquidus surface [8]. Most stainless-steel compositions are on the iron-rich side of ternary and contain less than 80% Fe. In order to predict the solidification sequence for the Fe-Cr-Ni ternary system using chromium and nickel equivalents, the Cr_{eq} and Ni_{eq}

indexes can be estimated with the following Equations ((1) and (2)) [4–6], where contents of elements are given in wt.%:

$$Ni_{eq} = Ni + 30\ C + 30\ N + 0.5\ Mn \quad (1)$$

$$Cr_{eq} = Cr + Mo + 1.5\ Si + 0.5\ Nb \quad (2)$$

The solidification mechanism of austenitic stainless steels, as predicted from the equivalence ratio Cr_{eq}/Ni_{eq}, can occur in accordance with one of the following four modes [2–4,7]:

$$\text{Austenite mode (A): } L \rightarrow L + \gamma \rightarrow \gamma \quad (3)$$

$$\text{Austenitic-Ferrite mode (AF): } L \rightarrow L + \gamma \rightarrow L + \gamma + \delta \rightarrow \gamma + \delta \quad (4)$$

$$\text{Ferrite-Austenite mode (FA): } L \rightarrow L + \delta \rightarrow L + \delta + \gamma \rightarrow \gamma + \delta \rightarrow \gamma \quad (5)$$

$$\text{Ferrite mode (F): } L \rightarrow L + \delta \rightarrow \delta \rightarrow \delta + \gamma \quad (6)$$

where L is the liquid phase, γ is the austenite, and δ is the ferrite.

The solidification of the cast microstructures at room temperature is primarily an austenitic mode (3), where there was primary austenite solidification without the appearance of ferrite, and an austenitic–ferritic mode (4), where the primary austenite solidification was followed by the nucleation and growth of ferrite with a eutectic reaction of the remaining inter-dendritic Cr-enriched liquid phase. With the ferrite-austenite mode (5) of solidification, primary ferrite precipitation followed on further cooling, with austenite formation in the three-phase region. This is a eutectic reaction. Below the solidus line, the ferrite transforms to austenite in the solid-state until it is completely dissolved. The ferrite mode (6) was primary ferrite solidification with austenite forming a structure along the ferrite boundaries upon cooling in the solid state [4]. At higher ratios of chromium over nickel, the microstructure at room temperature can retain considerable amounts of δ-ferrite, for example, in duplex stainless steels [8–10].

However, in real cases the solidification sequence also depends on the solidification rate, which influences the possible growth competition between the stable and metastable solid phases through the kinetic undercooling required for their growth. Variations in the solidification rate also impact the amount of ferrite and causes its increase or decrease, depending on the solidification sequence for the considered solidification rate [4,11–13].

Under the prevailing non-equilibrium solidification conditions, segregations alter the product phases and their compositions [8,14]. Accordingly, with the microstructure evolution in austenitic stainless steels, the interdendritic regions are slightly enriched in both Cr and Ni, while in the austenitic-ferritic mode there is significant enrichment in terms of Cr and the depletion of Ni. The ferrite nucleates in the Cr-enriched and Ni-weakened regions as a non-equilibrium phase. The segregations of Cr to ferrite and Ni to austenite during solidification play a major role in stabilizing the ferrite during the subsequent solid-state transformation [15,16].

The consequence of segregation at the boundaries of the dendrites is the mechanical instability of the steel during hot forming [17–19]. During the continuous casting of this steel at the casted slab/beam locations, where the cooling rate during casting is high enough, part of the metastable δ-ferrite is maintained at room temperature due to the imperfect transformation of the δ in γ [20–22]. Ferrite has a negative influence on the hot ductility [4]. In the majority of cases the δ-ferrite can be eliminated by annealing in the range between 1050 °C and 1250 °C with a sufficiently long time [4]. The annealing time at a certain temperature influences the amount and the shape of the δ-ferrite after annealing. Annealing dissolves and changes the shape [23–25] of the δ-ferrite.

The aim of the study was to determine the effectiveness of the transformation, i.e., the decomposition of the δ-ferrite crystal grains upon annealing at 1050 °C, 1150 °C and 1250 °C with respect to the amount and the shape of the δ-ferrite in SS2343 stainless steel. Studies on solid-state phase transformations related to the heat treatment of various

grades of stainless steels are especially important for understanding welding processes, in order to improve welding quality in terms of mechanical, metallurgical and corrosion properties [9,10,13–29].

2. Materials and Methods

The research was conducted on laboratory-scale SS2343 stainless steel. The SS2343 austenitic steel was melted in an induction furnace and then cast into an investment-casting mold. The dimensions of the cast ingots were 250 mm long × 40 mm wide × 20 mm tall. The chemical composition analyzed using a quantitative chemical analysis of steel (instruments used: ICP-AES Perkin Elmer (PerkinElmer, Waltham, MA, USA), Eltra CS800, Eltra ON (Eltra GmbH, Haan, Germany)) is given in Table 1.

Table 1. Chemical composition of SS2343 austenitic steel in wt.%.

Element	C	Si	Mn	Cr	Ni	Mo	Ti	Al	P	S	N
wt.%	0.023	0.75	1.52	17.4	10.8	2.62	0.005	0.009	0.052	0.017	0.0135
tolerance wt.%	±0.003	±0.02	±0.05	±0.2	±0.2	±0.05	±0.001	±0.001	±0.002	±0.002	±0.002

2.1. Sampling

The samples were taken from within the ingot. The specimens were cut 3 mm from the outer surface: (a) 10 mm from the outer surface, (b) and 20 mm from outer surface, and (c) the center of the ingot.

2.2. Annealing

The selected samples were then annealed in an air atmosphere in a Nabertherm furnace LT 9/11 (Nabertherm GmbH, Lilienthal, Germany). The annealing temperatures were 1050 °C, 1150 °C and 1250 °C, with soaking times of 5 and 40 min.

2.3. Metallographic Analyses

The metallographic samples were prepared by grinding with paper from P180 to P1200, polished with diamond and polish buff, and finally etched with aqua regia. Metallographic analyses of the microstructures were performed using optical microscopy (OM) with a Nikon mikrophot—FXA (Nikon, Tokyo, Japan).

In addition, scanning electron microscopy (SEM) and energy-dispersive spectroscopy (EDS) were used to analyze the chemical compositions of the samples (Jeol JSM-6500F (Jeol LTD., Tokyo, Japan), with an Inca Energy 450, detector type INCA X-SIGHT LN2 (Oxford Instruments, Abingdon, UK). The samples were analyzed with an accelerating voltage of 15.0 kV and an energy resolution of 10 eV.

The ferrite fractions were measured using a magnetic method, with a Fischer Feritscope MP30 (Helmut Fischer GmbH, Sindelfingen, Germany), which non-destructively (NDT) measures the ferrite content in range of 0.1% to 80% Fe or 0.1% to 95.5% FN (magnetic induction method) in austenitic or duplex stainless steels, with the uncertainty of the measurement being ±0.4 vol.%.

2.4. Thermodynamic Calculations

Thermodynamic calculations were performed with the Thermo-Calc software (version 2017a, Thermo-Calc Software AB, Solna, Sweden) [30] using database TCFE8 for steels/Fe-alloys V8.1. Phase equilibria for the composition (wt.%) of Fe-(16-24)Cr-0.023 C-0.75 Si-1.52Mn-10.8 Ni-2.62Mo-0.017S and the volume fractions of polymorphous equilibrium phases for the laboratory-prepared SS2343 stainless steel were calculated [11,12,29].

3. Results and Discussion

According to the chemical composition given in Table 1 and Equations (1) and (2), the Cr_{eq}/Ni_{eq} ratio is 1.62. Generally, for Cr_{eq}/Ni_{eq} in the range $1.48 < Cr_{eq}/Ni_{eq} < 1.95$, δ-ferrite is the primary phase and austenite is also formed with a peritectic reaction in the two-phase region (eutectic) of solidification. Phase equilibria for the composition (wt.%) of Fe-(16-24)Cr-0.023C-0.75Si-1.52Mn-10.8Ni-2.62Mo-0.017S were calculated in the temperature range 400–1600 °C and the results are presented in the form of a vertical section of the phase diagram in Figure 1. In the vertical section of the phase diagram, ten areas corresponding to the equilibria are illustrated, while ten phases of equilibrium exist. The phase equilibrium consist of f.c.c. (austenite), b.c.c. (δ-ferrite), M23C6 carbides, and the intermetallic σ sigma phase and χ chi phase.

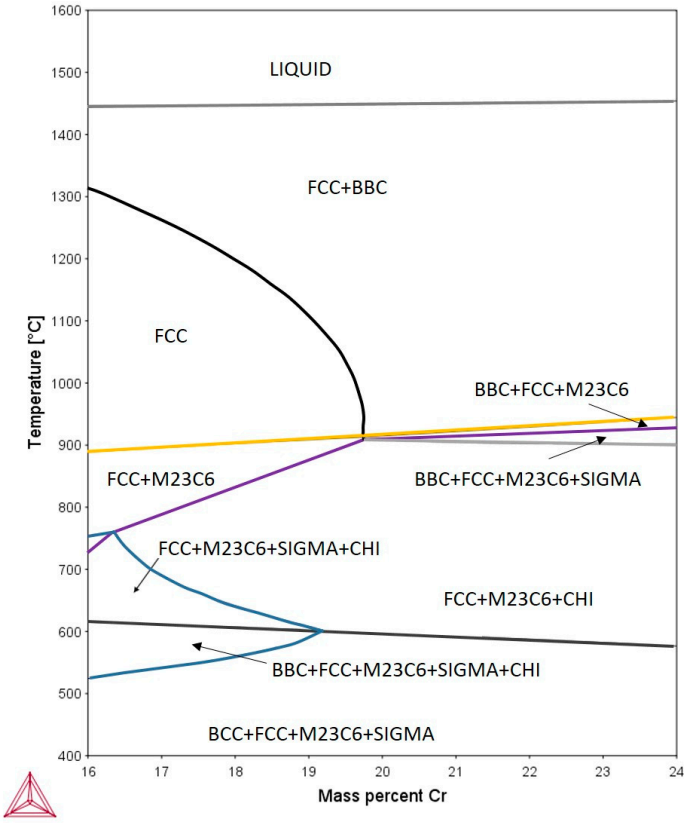


Figure 1. Vertical section of the phase diagram predicted for the Fe-(16-24)Cr-0.023C-0.75Si-1.52Mn-10.8Ni-2.62Mo-0.017S system.

The volume fractions of polymorphous equilibrium phases were predicted [30] for the composition Fe-17.4Cr-0.023C-0.75Si-1.52Mn-10.8Ni-2.62Mo-0.017S in wt.% (SS2343 steel) in the temperature range 700–1500 °C (Figure 2). Delta ferrite (δ) is a high-temperature version of ferrite formed during the solidification of austenitic stainless steels. It is an undesirable phase because it can form sigma phase (σ) [11,28]. The σ-phase is an intermetallic compound with iron and chromium; it is hard and brittle and can cause various problems during the hot forming of steels. Moreover, it also increases the tendency for pitting corrosion [1]. The M23C6 carbides are chromium-based, but they also contain a small proportion of tungsten, molybdenum, vanadium and iron.

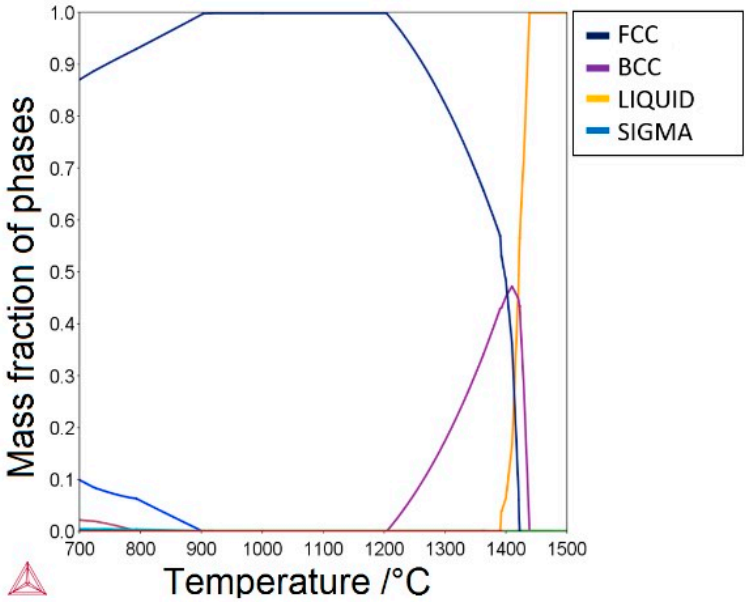


Figure 2. Calculated volume fractions of phases for SS2343 stainless steel depending on the temperature.

The thermodynamic calculation revealed stable δ-ferrite in the temperature range 1205–1438 °C. The highest volume fraction of this phase, about 47%, is predicted for temperatures between 1400 °C and 1419 °C. The measured content of δ-ferrite in an as-cast ingot of SS2343 stainless steel lies between 10.7% and 14.6 vol.%, where the amount of δ-ferrite is slightly lower at the surface of the ingot, due to the higher rate of cooling. The δ-ferrite fraction content (vol.%) in the as-cast ingot is, on average, 12.51 vol.%. The ferrite content after annealing decreases with a higher annealing temperature and with a longer annealing time. At a temperature of 1150 °C, for 5-and 40-min annealing times, we have minimum amounts of δ-ferrite of 5.07 and 2.64 vol.%, respectively. With further increasing of the annealing temperatures, the vol.% of ferrite increases again. At 1250 °C for 5 or 40 min of annealing time, the measured δ-ferrite content is 6.17 and 5.52 vol.%, respectively. From Figure 2, one can see that under equilibrium conditions at 1250 °C, there is about 8% ferrite present.

From estimates of both the as-cast and the annealed percentages of δ-ferrite, f/fo vs. time can be plotted for each heat of annealing. Here, f/fo is the fraction of the ferrite remaining and time refers to the actual amount of time in the furnace. F_0 is the initial content of ferrite (as-cast state), f is the content at a certain time and annealing temperature. The plots for the various temperatures and for 5- and 40-min annealing times can be seen in Figure 3. The line dissolution of δ-ferrite in each case is at the best location, which was determined using linear regression. The largest reduction of δ-ferrite was achieved at 1150 °C.

The delta-ferrite microstructure-morphology in the cast structure and the transformation during heat treatment are shown in Figures 4 and 5. A series of photographs was taken. The microstructure of the as-cast state of the SS2343 stainless steel and the typical morphology of δ-ferrite at sub-surface (a), intermediate (b), and center of the ingot (c) are shown in Figure 4. A typical evolution of the morphology of the δ-ferrite microstructure after 5 min annealing at 1050 °C, 1150 °C and 1250 °C is shown in Figure 5.

In the as-cast microstructure close to edge (Figure 4a) there is the skeletal ferritic network (vermicular), and at the center it becomes a lathy (Figure 4c), finer structure. The vermicular is aligned skeletal network. Their orientation is along the heat flow direction. The ferrite present is the remnants of the primary and dendrite arms. The lacy morphology is characterized by an interlaced ferrite network oriented along the growth direction. The acicular morphology is a random arrangement of needle-like ferrite distributed in

an austenite matrix. The final morphology is globular morphology. It is characterized by ferrite in globules which are randomly distributed in a matrix of austenite.

After annealing at 1050 °C (Figure 5a–c), single partially enclosed residues of ferritic networks (lathy) are detected. In the case of 5 min of annealing at 1150 °C (Figure 5d–f), the ferritic network is no longer seen. There was reduction in the ferrite's volume fraction observed and increase in the average size (acicular shape) and the roundness of the ferrite. After annealing at 1250 °C (Figure 5g–i), the ferrite volume fraction increased in terms of the size of the individual ferrite island and the change of its shape to more spherical. With a higher temperature of annealing, a reduction of the ferrite volume fraction and ferrite spheroidization are pronounced. In the microstructures, the bright background is the austenitic matrix, while the dark phases represent δ-ferrite.

In Figure 5, showing the progress of δ-ferrite dissolution, the images to the left part of each of these figures are of the vermicular structure, which is located along the surface of the specimen or ingot. The lathy ferrite structure becomes located in the center regions of the ingot. It appears that the pools of δ-ferrite simply dissolved as the heat treatment took place. It seems that an amount of spheroidization did take place, especially in the final stages. It appears that the vermicular structure developed in the dissolution process at a slightly higher rate than did the lacy structure. These observations are in good agreement with previous studies [25,31–34]. During the dissolution process the various morphologies of the ferrite tend to lose their elongated shapes and move toward spheric ones. This softening of the ferrite phase may consequently produce beneficial mechanical properties [35].

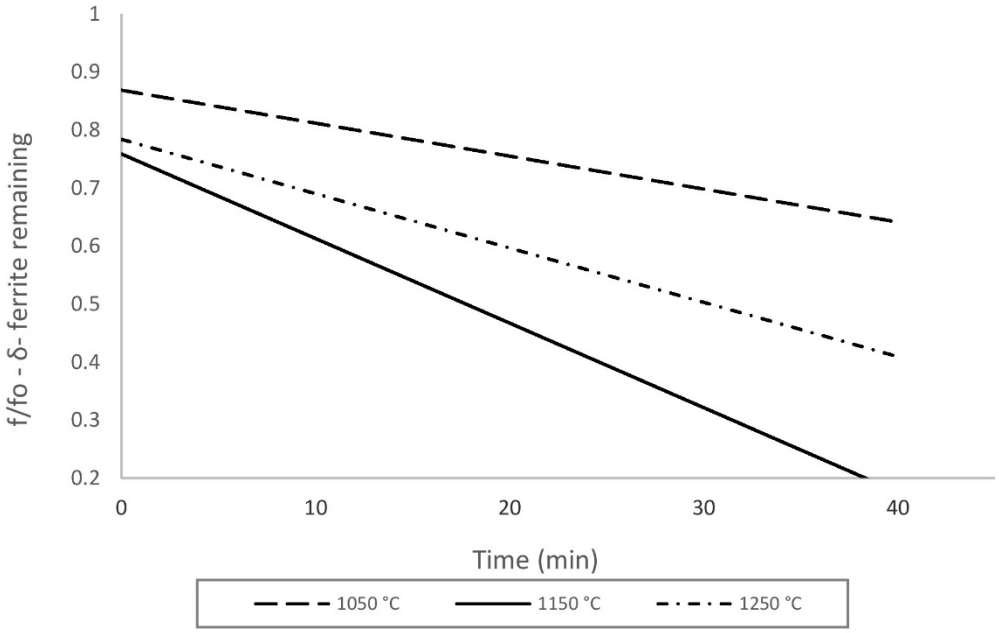


Figure 3. Comparison of the ferrite dissolution data for various heat treatments of SS2343 stainless steel.

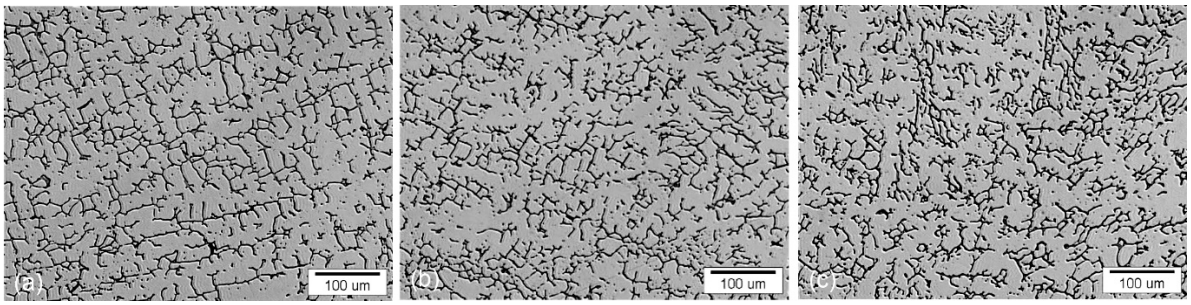


Figure 4. Optical micrographs of δ-ferrite in the as-cast microstructure. Locations are 3 mm (**a**), 10 mm from edge (**b**), and center of the ingot (**c**).

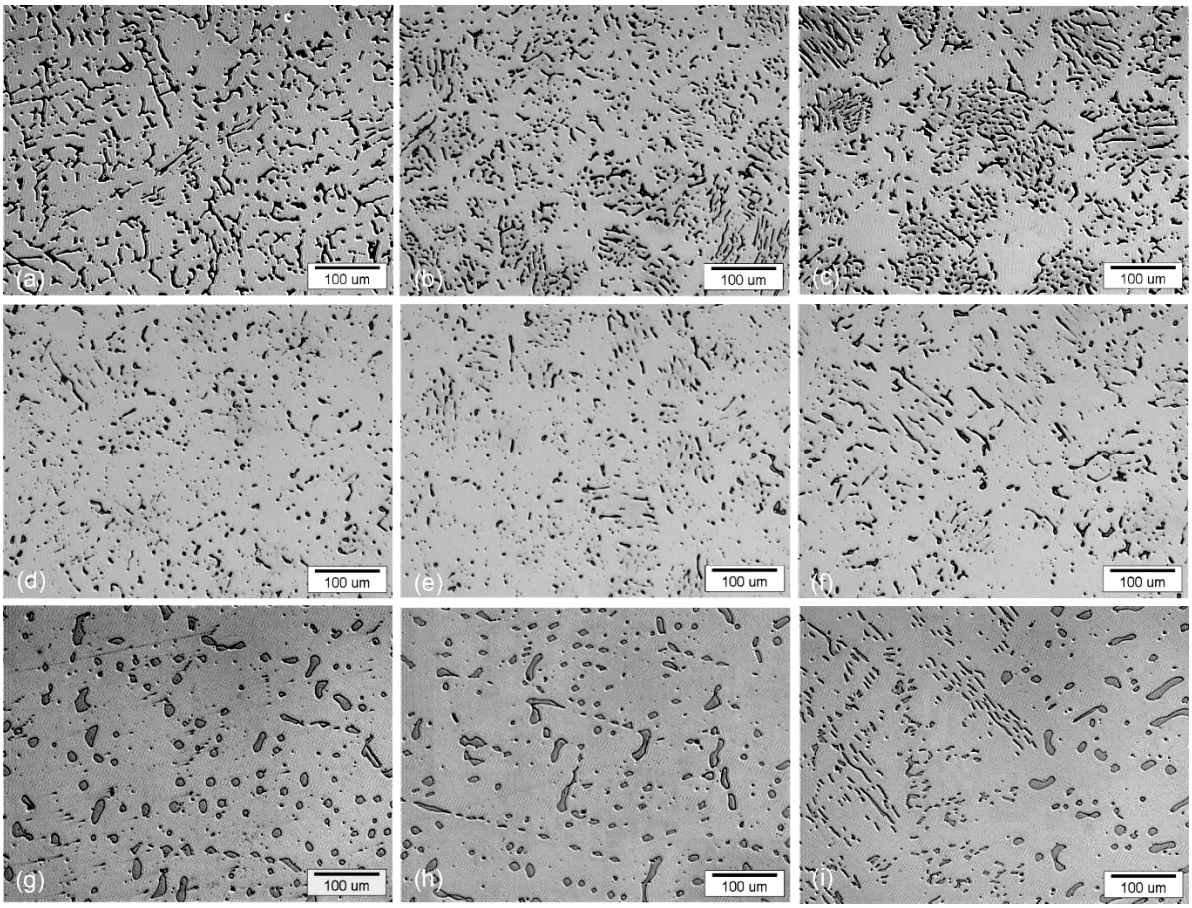


Figure 5. Evolution of morphology of δ-ferrite in microstructure after 5 min annealing at 1050 °C (**a**–**c**), 1150 °C (**d**–**f**), and 1250 °C (**g**–**i**). Locations are 3 mm (**a**,**d**,**g**), 10 mm from the edge (**b**,**e**,**h**), and center of the ingot (**c**,**f**,**i**).

Microstructural changes taking place during the heat treatment of stainless steel are complex [23]. A visual assessment of the specimen's microstructure suggests some differences, both in terms of the morphology and the distribution of the ferrite. In general, an elevated-temperature treatment leads to the dissolution of the metastable ferrite [23]. In addition, it was noticed that the dendritic network of the ferrite breaks down and tends to spheroidize. After annealing, a reduction of the ferrite content is observed, and accompanied by an increase in the size of the individual ferrite islands and a change in shape to more spherical. The difference in the free-energy levels of the metastable ferrite and the stable transformation products acts as the driving force for the dissolution process. As a result of the spheroidization process, the ratio of the surface area to volume of the ferrite particles decreases considerably, and this leads to a net reduction in the interfacial energy [23]. This can provide some advantages with regard to the crack-initiation property of the material [24].

Significant differences in the chemical composition that exist in the solute concentrations of the ferrite and austenite phases were identified. It is expected that such compositional inhomogeneities stemming from non-equilibrium solidification would disappear with heat treatments at high temperatures. SEM/EDS analyses demonstrate (see Figure 6, and Table 2) that the ferrite phase of the cast microstructure is enriched in chromium and molybdenum and depleted in nickel.

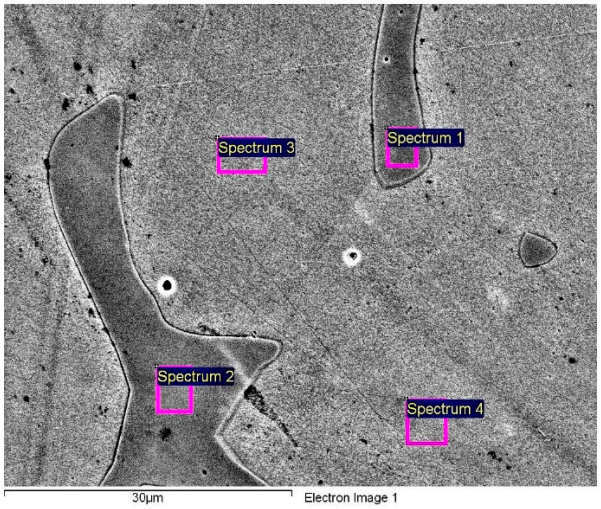


Figure 6. A representative SEM–EDS analysis of as-cast microstructure of SS2343 stainless steel.

Table 2. EDS results in wt.% of the analyzed δ-ferrite (spectra 1, 2) and austenite (spectra 3, 4) in as-cast microstructure of SS2343 stainless steel.

Spectrum	Si	P	S	Cr	Mn	Fe	Ni	Mo
1	0.40	0.00	0.00	25.37	1.62	63.14	4.25	5.21
2	0.47	0.13	0.00	24.73	1.40	63.92	4.84	4.51
3	0.46	0.00	0.23	18.40	1.76	68.36	9.48	1.30
4	0.44	0.00	0.00	17.92	1.48	67.95	10.51	1.70

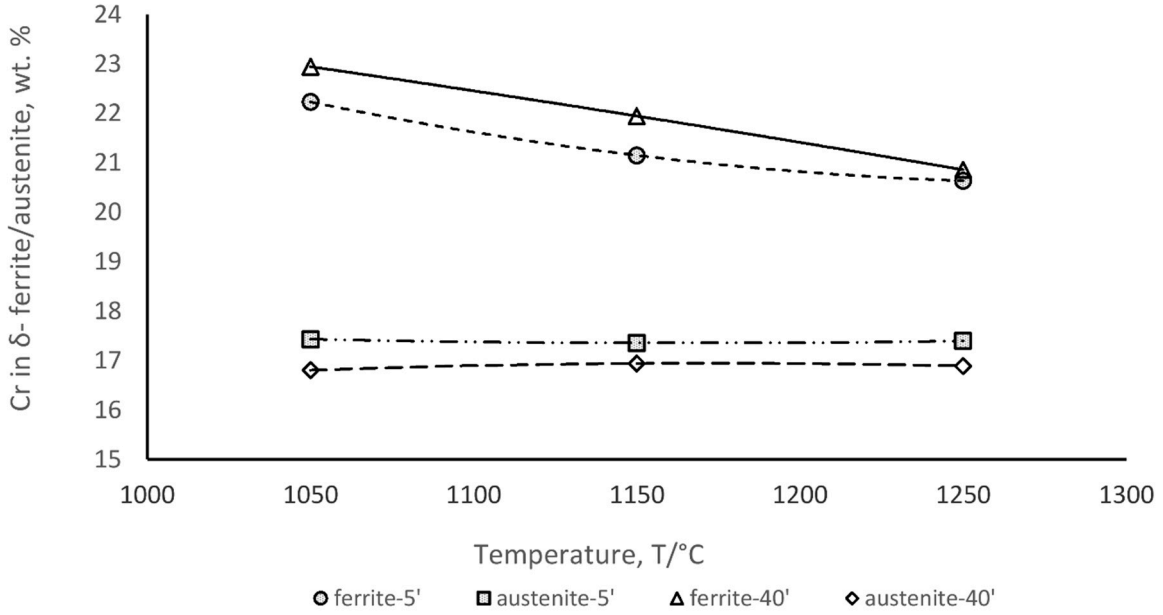
The contents of chromium, nickel and molybdenum in wt.%, and their distribution between the δ-ferrite and austenite with respect to the temperature and time of annealing for the SS2343 stainless steel are shown in Figures 7 and 8. The annealing times were 5 min and 40 min. The δ-ferrite is enriched with chromium and molybdenum, while it is depleted in nickel, irrespective of the temperature and the annealing time. It is believed that such compositional inhomogeneities stem from the non-equilibrium solidification. It is worth noting that the electron beam size in the EDS analysis is smaller than ferrite grains. Such an analyzed volume does not detect the austenitic grains.

Significant differences exist in the solute concentrations of the ferrite and austenite phases. Figure 7 shows that for the same annealing time, the chromium content in the δ-ferrite decreases slightly at higher temperatures. However, the chromium content in δ-ferrite is slightly higher for an annealing of 40 min. Molybdenum behaves similarly. However, the nickel content in the δ-ferrite increases with a higher temperature and a longer annealing time.

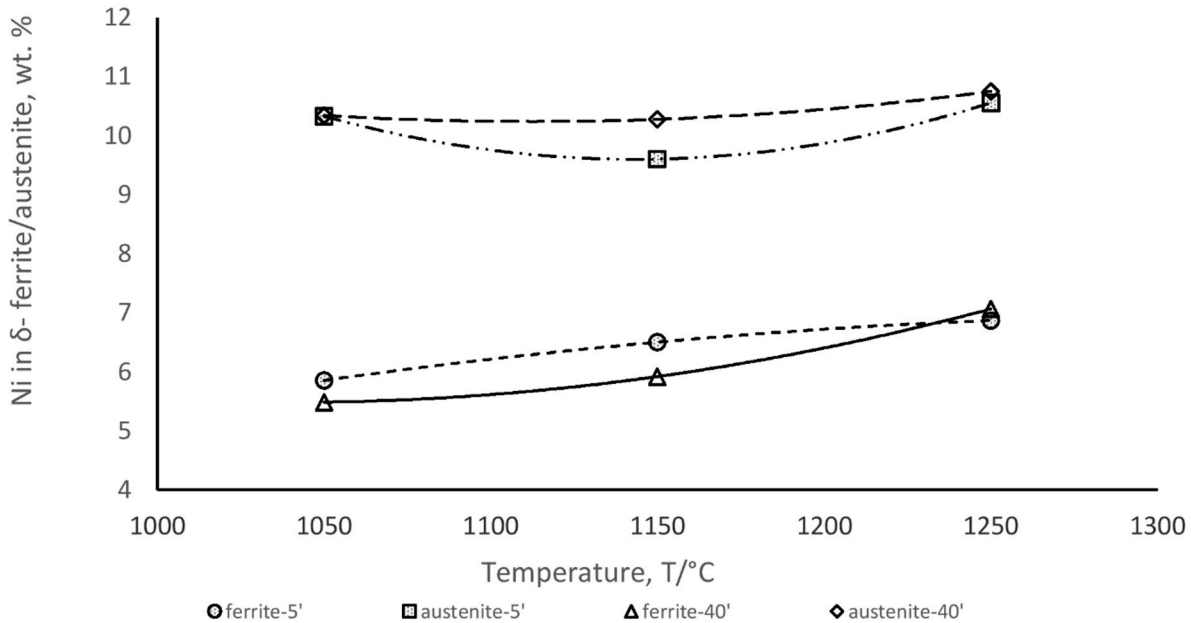
The chemical composition of the austenite is almost independent of the temperature and annealing time. The deviations of the measured contents of chromium, nickel and molybdenum are much lower in the δ-ferrite than in the austenite for an annealing time of 40 min. In Figure 8 are presented the cumulative concentrations of the elements Cr, Ni and Mo in the matrix of austenitic stainless steel, particularly for the individual changes in the concentrations of Cr, Ni and Mo in the ferrite and austenite. The cumulative for Cr is calculated as $Cr_{Vol.\%.cum} = (V_A * Cr_{Vol.\%.A} + V_F * Cr_{Vol.\%.F})/100$, where V_A and V_F are volume fractions of ferrite and austenite and $V_A + V_F = 100$. Cumulative for Ni and Mo are calculated in the same way. The curves are held on the side of the austenite, because the proportion of austenite is increasing from 87.5% in the as-cast state to 93.1% or 94.5% in the annealed state.

Microstructural changes after annealing revealed that the ferrite phase, originally present in a dendritic morphology, tends to break up and spheroidize. The δ-ferrite morphology varies from vermicular, lacy and acicular shapes to globular for higher tem-

peratures and for longer exposure times, since the temperature and time are important for diffusion processes. The two morphologies present in the as-cast microstructure both tend to progress to a spheroidized morphology. In the δ-ferrite after annealing, concentrations of Cr and Mo decrease, and conversely the concentration of Ni increases. All by small, but significant, amounts. The dissolution process is interface diffusion controlled at δ-γ interfaces. The Cr depletion in ferrite increases its instability and enhances its dissolution. Dissolution kinetics was controlled by volume diffusion of Cr, Ni and Mo [23,33].

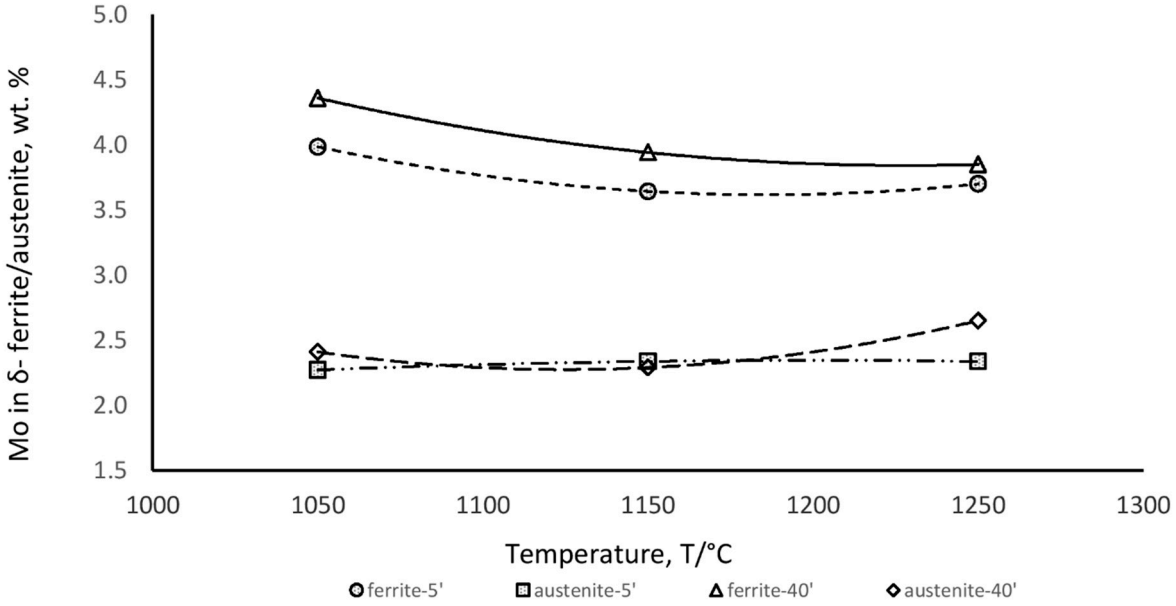


(**a**)



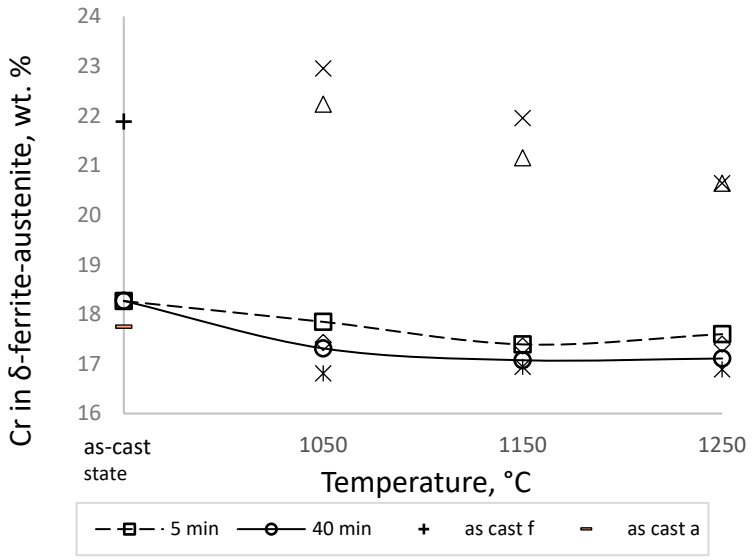
(**b**)

Figure 7. *Cont*.



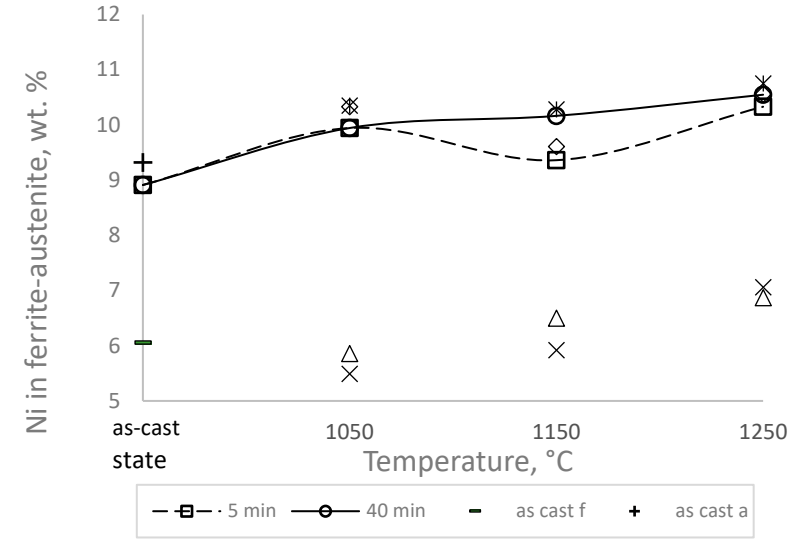
(**c**)

Figure 7. Content of chromium (**a**), nickel (**b**) and molybdenum (**c**) in the δ-ferrite and austenite depends on the temperature and time of annealing for the SS2343 stainless steel.

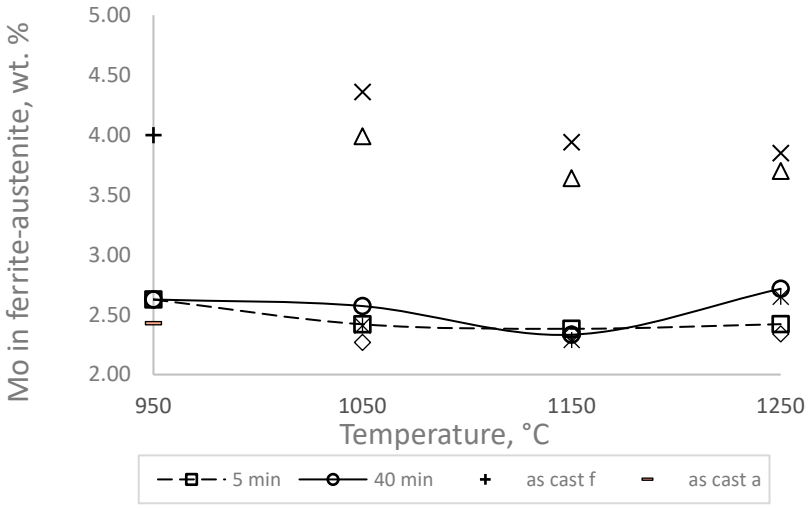


(**a**)

Figure 8. *Cont*.



(**b**)



(**c**)

Figure 8. Distribution and cumulative concentrations of chromium (**a**), nickel (**b**) and molybdenum (**c**) in the δ-ferrite -**f**- and austenite -**a** after annealing for 5 or 40 min; concentration markers: Δ 5 min f, × 40 min f, ◊ 5 min a, ∗ 40 min a.

The nature of the compositional changes is closely related to the specific sequence of transformations that the ferrite phase undergoes before its final disappearance. The former process would require that any compositional differences between the ferrite and the austenite phases would diminish during heat treatment, resulting in homogenization with the austenite matrix. The latter reaction would cause these compositional differences to either be sustained or marginally enhanced [23]. This is probably what has happened for chromium, molybdenum and nickel in the ferrite in this case. The observed changes in the solute concentration could be explained as being the result of the transformation of ferrite into austenite and sigma phases [23].

Most of the scientific literature on δ–ferrite dissolution states that increasing annealing time and temperature promote the dissolution of δ–ferrite. Our study on δ–ferrite dissolution of austenitic stainless SS2343 has shown, that at 1250 °C δ–ferrite fraction is increasing when compared to lower annealing temperatures and shorter annealing times. This is contradictory to the existing literature [31–34] except to the results reported by Saied on Fe-Cr-Ni austenitic steel [4]. Results of his study clearly show that for the studied Fe-Cr-Ni austenitic steel δ–ferrite dissolution is not decreasing with increasing

annealing temperature and time. In his study it is clearly shown, that with annealing temperatures above 1280 °C (regardless of annealing time), the content of δ–ferrite increases. Furthermore, first increases in δ–ferrite content is detected as low as at 1200 °C. One can conclude, that the δ–ferrite dissolution dynamically depends on both, temperature and time. A widely accepted assumption, that δ–ferrite dissolution process increases with increasing annealing temperature and time thus seems not to be optimal, at least for the Fe-Cr-Ni austenitic steel studied by Saied [4].

In our study, austenitic stainless steel SS2343 has significantly different chemical composition compared to Fe-Cr-Ni austenitic steel studied by other authors e.g., [4,31–34]. Based on comparison of Saied [4], and experimentally obtained data of our study, it can be concluded that (1) δ–ferrite dissolution is not monotonically decreasing with increasing annealing temperature and time, and (2) that the δ–ferrite dissolution should be carefully studied for every individual alloy. Furthermore, equilibrium (better transient) values of δ–ferrite seems to change or depend (as function of annealing temperature and time) on chemical composition of base alloy. And that was the purpose of present study—determination of δ–ferrite dissolution of the SS2343.

4. Conclusions

The solidification behaviors of laboratory cast austenitic SS2343 stainless steel in terms of the volume fraction of δ-ferrite in the as-cast state and the transformation after subsequent annealing were investigated in the temperature range from 1050 °C to 1250 °C. It solidifies in the ferrite-austenite mode (FA), where the formation of the austenite takes place following the primary ferrite. With further cooling at room temperature, a large amount of ferrite is consumed by the austenite as part of a diffusion-controlled solid-state transformation. After annealing, the volume of δ-ferrite is decreasing when increasing the temperature and time of the annealing.

- After annealing at 1150 °C at 5 and 40 min, the content of δ-ferrite was reduced to 5.0 and 2.64 vol.%, respectively. Thus, about 60% or 80% the δ-ferrite is transformed by annealing.
- After annealing at 1150 °C, the δ-ferrite dissolution and transformation process initiates in secondary arms and progresses also in primary arms, where dendritic network of δ-ferrite tends to break down and spheroidize.
- After annealing at 1250 °C, the dissolution of δ-ferrite was only ~50%. Morphologically is remaining δ-ferrite mostly spherical.
- Concentrations of Cr, Ni and Mo in the δ-ferrite during annealing are diffusion controlled and are approaching toward concentrations in matrix of SS2343.

Author Contributions: Conceptualization, B.A., F.V. and F.T.; methodology, B.A., F.V. and F.T.; software, F.V.; validation, B.A., F.V. and F.T.; formal analysis, B.A., F.V. and F.T.; investigation, B.A. and F.T.; resources, F.T.; writing—original draft preparation, B.A. writing—review and editing, F.T.; supervision, F.T.; funding acquisition, F.T. All authors have read and agreed to the published version of the manuscript.

Funding: This research was performed at the public research institute IMT, Ljubljana, Slovenia, in the frame of research program no. P2-0050. The Slovenian Research Agency is acknowledged for its financial support of the research core funding of P2-0050.

Institutional Review Board Statement: Not applicable.

Informed Consent Statement: Not applicable.

Conflicts of Interest: The authors declare no conflict of interest.

References

1. Davis, J.R. *Stainless Steels. ASM Specialty Handbook*; ASM International: Geauga County, OH, USA, 1994.
2. Steiner Petrovič, D.; Klančnik, G.; Medved, J. Differential scanning calorimetry study of the solidification sequence of austenitic stainless steel. *J. Anal. Calorim.* **2011**, *105*, 251–257. [CrossRef]

3. Martorano, M.A.; Tavares, C.F.; Padilha, A.F. Predicting delta ferrite content in stainless steel castings. *ISIJ Int.* **2012**, *6*, 1054–1065. [CrossRef]
4. Saied, M. *Experimental and Numerical Modeling of the Dissolution of Delta Ferrite in the Fe-CR-N System: Application to Austenitic Stainless Steels*; English. NNT: 2016GREAI016; Université Grenoble Alpes: Saint-Martin-d'Hères, France, 2016.
5. Fu, J.W.; Yang, Y.S.; Guo, J.J.; Ma, J.C.; Tong, W.H. Microstructure evolution in ASI304 stainless steel during near rapid directional solidification. *Mater. Sci. Technol.* **2009**, *25*, 1013–1016. [CrossRef]
6. Plaut, R.L.; Herrea, C.; Escriba, D.M.; Rios, P.R.; Padilha, A.P. A short review on properties and performance, wrought austenitic stainless steels at high temperatures: Processing, microstructure. *Mater. Res.* **2007**, *10*, 453–460. [CrossRef]
7. Padilha, A.F.; Tavares, C.F. Delta ferrite formation in austenite stainless steel. *Mater. Sci. Forum* **2013**, *730–732*, 733–738.
8. Shankar, V.; Gill, T.P.S.; Mannan, S.L.; Sundarsan, S. Solidification cracking in austenitic stainless steel welds. *Sadhana* **2003**, *28*, 359–382. [CrossRef]
9. Inoue, H.; Koseki, T. Clarification of solidification behaviors in austenitic stainless steels based on welding process. *Nippon Steel Tech. Rep.* **2007**, *95*, 62–70.
10. Inoue, H.; Koseki, T. Solidification mechanism of austenitic stainless solidified with primary ferrite. *Acta Mater.* **2017**, *124*, 430–436. [CrossRef]
11. Janovec, J.; Šuštaršič, B.; Medved, J.; Jenko, M. Phases in austenitic stainless steels. *Mater. Tehnol.* **2003**, *37*, 307–312.
12. Andersson, J.O.; Helander, T.; Höglund, L.; Shi, P.; Sundman, B. Termo-calc DICTRA, computational tool for materials science. *Calphad* **2002**, *26*, 273–312. [CrossRef]
13. Calliari, I.; Breda, M.; Gennari, C.; Pezzato, L.; Pellizzari, M.; Zambon, A. Investigation on solid-state phase transformation in a 2510 duplex stainless steel grade. *Metals* **2020**, *10*, 967. [CrossRef]
14. Koseki, T.; Flemings, M.C. solidification of undercooled Fe-Cr-Ni alloys part II-microstructural evolution. *Metall. Mater. Trans.* **1996**, *27*, 3226–3240. [CrossRef]
15. Tümer, M.; Yilmaz, R. Characterization of microstructure, chemical composition and toughness of multipass welded joint of austenitic stainless steel AISI 316L. *Int. J. Adv. Manuf. Technol.* **2016**, *87*, 2567–2579. [CrossRef]
16. Laxminarayana, P.; Chennaksava Reddy, A. Quantification of delta ferrite in austenitic stainless steel cast investments shell moulds. In Proceedings of the 4th National Conference on Materials and Manufacturing Processes, Hyderabad Pradesh, India, 8–9 August 2008; pp. 62–65.
17. Scheller, P.R.; Bleck, W.; Flesch, R. Effect of residual elements on hot-crack susceptibility of austenitic stainless steel. *Steel Res. Int.* **2004**, *75*, 672–679. [CrossRef]
18. Jang, A.Y.; Lee, D.J.; Lee, S.H.; Shim, J.H.; Kang, S.W.; Lee, H.W. Effect of Cr/Ni equivalent ratio on ductility-dip cracking in AISI 316L weld metals. *Mater. Des.* **2011**, *32*, 371–376. [CrossRef]
19. Argains-Juarez, C.R.; Vazuez, A.; Garza-Montes-de-Oca, N.F.; Colas, R. Sensitization of austenitic stainless steel due to the occurrence of δ-ferrite. *De Gruyter Corros. Rev.* **2018**, *37*, 179–186. [CrossRef]
20. Mateša, B.; Samardžič, I.; Dunder, M. The influence of heat treatment on delta ferrite transformation in austenitic stainless steel welds. *Metalurgija* **2012**, *51*, 229–232.
21. Kobayashi, S.; Sowada, K.; Hara, T.; Kushima, H.; Kimura, K. The formation and dissolution of residual δ-ferrite in ASME grade 91. *Mater. Sci. Eng. A* **2014**, *592*, 241–248. [CrossRef]
22. Sasikala, G.; Ray, S.L.; Mannan, S.L. kinetic of transformation of delta ferrite during creep in a type 316(N) stainless steel weld metal. *Mater. Eng. A* **2003**, *359*, 86–90. [CrossRef]
23. Raghunathan, V.S.; Seetharaman, V.; Venkadesan, S.; Rodriquez, P. The influence of post weld heat treatments on structure, composition and amount of ferrite in type 316 stainless steel welds. *Metall. Trans. A* **1979**, *10A*, 1683–1689. [CrossRef]
24. Cho, J.Y.; Czerwinski, F.; Szpunar, J.A. The effect of reheating condition on ferrite content in austenitic stainless steel slabs. *J. Mater. Sci.* **2000**, *35*, 1997–2003. [CrossRef]
25. Gokovič-Gekič, A.; Avdušinovič, H.; Hodžč, A.; Mandžuka, E. Effect of temperature and time on decomposition of δ-ferrite in austenitic stainless steel. *Rmz-MG* **2020**, *67*, 65–72. [CrossRef]
26. Ciuffini, A.F.; Barella, S.; Di Cecca, C.; Gruttadauria, A.; Mapelli, C.; Mombelli, D. Isothermal austenite–ferrite phase transformations and microstructural evolution during annealing in super duplex stainless steels. *Metals* **2017**, *7*, 368. [CrossRef]
27. Gruttadauria, A.; Barella, S.; Mapelli, C.; Mombelli, D. Influence of different soaking times at 1050 °C on UT response due to microstructure evolution of 2205 duplex stainless steel. *Metals* **2020**, *10*, 503. [CrossRef]
28. Marin, R.; Combeau, H.; Zollinger, J.; Dehmas, M.; Rouat, B.; Lamontagne, A.; Loukashenko, N.; Lhenry-Robert, L. σ-phase formation in super austenitic stainless steel during directional solidification and subsequent phase transformations. *Met. Mater. Trans. A* **2020**, *51*, 3526–3534. [CrossRef]
29. Bermejo, M.A.V.; Wessman, S. Computational thermodynamics in ferrite content prediction of austenitic stainless steel weldments. *Weldments World* **2019**, *63*, 627–635. [CrossRef]
30. ThermoCalc Software Package. 2017. Available online: https://thermocalc.com (accessed on 11 January 2021).
31. Allahyari, A.A.; Farhangi, H.; Hadavi, S.M.M. Investigation of aging heat treatment on microstructure and mechanical properties of 316L austenitic stainless steel weld metal. *Wit Trans. Eng. Sci.* **2005**, *51*, 63–71.
32. Arnaldo, F.J.; Jorge, O.; Rodrigo, M. Ferrite quantification methodologies for methodologies for duplex stainless steel. *J. Aerosp. Technol. Mang. São José Dos Campos.* **2016**, *8*, 357–362.

33. Kim, S.H.; Moon, H.K.; Kang, T.; Lee, C.S. Dissolution kinetics of delta ferrite in AISI 304 stainless steel produced by strip casting process. *Mater. Sci. Eng.* **2003**, *A356*, 390–398. [CrossRef]
34. Gokul, O.S.; Byeong, S.K.; Ho, J.L.; Changheui, J. Evaluation of the thermal aging of δ-ferrite in austenitic stainless steel welds by electrochemical analysis. *Sci. Rep.* **2018**, *8*, 1–17.
35. Ratke, P.D. Study of the Effects of Heat Treatment on Delta-ferrite in Cast Austenitic Stainless Steel. Master's Thesis, Oklahoma State University, Stillwater, OK, USA, 1988. Available online: https://hdl.handle.net/11244/15698 (accessed on 9 April 2021).